JGR Atmospheres

RESEARCH ARTICLE
10.1029/2021JD034587

A Preliminary Study on the Organizational Modes of Mesoscale Convective Systems Associated With Warm-Sector Heavy Rainfall in South China

Sa Li[1], **Zhiyong Meng**[1], **and Naigeng Wu**[2]

[1]Department of Atmospheric and Oceanic Sciences, School of Physics, Peking University, Beijing, China, [2]Key Laboratory of Regional Numerical Weather Prediction, Institute of Tropical and Marine Meteorology, Chinese Meteorological Administration, Guangzhou, China

Key Points:

- The top three modes of the target mesoscale convective systems (MCSs) are the nonlinear mode (NL) and two dominant linear modes: trailing (TS) and no (NS) stratiform rain
- NL systems develop faster, move more slowly, have shorter lifespans, and produce stronger 3-h and 6-h rainfalls than TS and NS systems
- The Total Totals index (TTI) is significantly different among the top three modes of the target MCSs

Correspondence to:
Z. Meng,
zymeng@pku.edu.cn

Citation:
Li, S., Meng, Z., & Wu, N. (2021). A preliminary study on the organizational modes of mesoscale convective systems associated with warm-sector heavy rainfall in South China. *Journal of Geophysical Research: Atmospheres*, *126*, e2021JD034587. https://doi.org/10.1029/2021JD034587

Received 13 JAN 2021
Accepted 2 AUG 2021

Author Contributions:
Conceptualization: Zhiyong Meng
Data curation: Sa Li, Zhiyong Meng, Naigeng Wu
Formal analysis: Sa Li, Zhiyong Meng
Funding acquisition: Zhiyong Meng
Investigation: Sa Li, Zhiyong Meng
Methodology: Sa Li, Zhiyong Meng
Project Administration: Zhiyong Meng
Resources: Zhiyong Meng, Naigeng Wu
Software: Sa Li
Supervision: Zhiyong Meng
Validation: Zhiyong Meng
Visualization: Sa Li, Zhiyong Meng
Writing – original draft: Sa Li
Writing – review & editing: Sa Li, Zhiyong Meng, Naigeng Wu

Abstract This work examines the organizational modes of mesoscale convective systems (MCSs) associated with warm-sector heavy rainfall events in South China based on composite radar reflectivities during April–June from 2007 to 2020. The results showed that these MCSs can be classified into the nonlinear mode (NL) and eight linear modes: trailing stratiform precipitation (TS), no stratiform precipitation (NS), leading stratiform precipitation (LS), parallel stratiform precipitation (PS), embedded lines (EL), bow echoes (BE), training line/adjoining stratiform (TL/AS), and multiple rain bands (MRB). The NL mode accounts for 40% of the total, while linear modes account for 60%, with the TS mode being the most frequent linear mode. The detailed features of the top three most frequent organizational modes (NL, TS, and NS) were examined in this work. First, the MCSs of the top three organizational modes have different formation modes. Eighty-four percent of NL systems and 77% of TS systems form via the broken areal mode, while 83% of NS systems form via the broken line mode. Second, relative to TS and NS systems, NL systems develop faster and have shorter lifespans but slower movements with higher 3-h and 6-h maximum precipitation values. Third, environmental analysis indicates that the Total Totals index (TTI) is significantly different among all the top three organizational modes, with the highest value in TS mode and the lowest value in NS mode. These features are apparently different from their counterparts in central East China due to different synoptic environments.

1. Introduction

Warm-sector heavy rainfall mostly occurs during the presummer rainy season (April–June), hundreds of kilometers ahead (to the south) of a surface front, or without a surface front (Ding, 1994; Huang et al., 1986). They sometimes occur in the confluence zones of southwesterly and southeasterly flows or in southwesterly flows without conspicuous convergence. Warm-sector heavy rainfall is mostly produced by mesoscale convective systems (MCSs; He et al., 2016) and thus, is generally characterized by localized areas, concentrated timespans, and high rainfall intensities (Lin, 2006), which may cause severe flooding and enormous losses of life and property. Relative to the generally low quantitative precipitation forecast (QPF) skill of rainfall where MCSs occur, as revealed in real-time statistics (https://www.wpc.ncep.noaa.gov/html/hpcverif.shtml) and in many studies (e.g., Squitieri & Gallus, 2016), the QPF skill is even lower for warm-sector heavy rainfall in South China, which is influenced by weakly synoptic-scale baroclinic forcing, land-sea contrasts, and complex terrain and has been the region representing the biggest challenge in heavy rainfall forecasting (Luo, 2017; Luo et al., 2017; Wu, Ding et al., 2020; Wu, Zhuang et al., 2020; Zhang and Meng, 2019). The organizational modes of MCSs associated with warm-sector heavy rainfall are key factors in determining the distribution and evolution of warm-sector heavy rainfall in South China, which however has not received adequate attention.

There have been numerous studies in the literature on the classification of the organizational modes of MCSs using radar data (e.g., Blanchard, 1990; Bluestein & Jain, 1985; Jirak et al., 2003; Loehrer & Johnson, 1995; Parker & Johnson, 2000; Wang, Cui, et al., 2014; Yang and Sun, 2018; Zheng et al., 2013). The common method for categorizing organizational modes is to examine the arrangement of the convective and stratiform rainfall regions of a given MCS. Earlier works on the organizational modes of MCSs mainly focused on squall lines or quasilinear MCSs. Parker and Johnson (2000) proposed three linear organizational

modes that occurred over the central United States during May in 1996 and 1997, including trailing stratiform precipitation (TS), leading stratiform precipitation (LS), and parallel stratiform precipitation (PS), with the TS mode having the highest frequency. Meng et al. (2013) found that the percentages of squall lines with different organizational modes in East China were consistent with the results found for squall lines over the central United States.

The organizational modes of general rather than just quasilinear MCSs have been examined over central East China (Zheng et al., 2013) and the Yangtze River basin (Wang, Cui, et al., 2014). Zheng et al. (2013) classified MCSs over central East China from June to September during 2007–2010 into a nonlinear (NL; accounting for 44.7% of the total MCSs) and six linear organizational modes, including no stratiform precipitation (NS), TS, LS, PS, bow echoes (BE), and embedded lines (EL). Similar to what was observed over central East China, a slightly smaller number of nonlinear MCSs relative to linear MCSs were found over the Yangtze River basin from June to July during 2010–2012, including TS, LS, PS, training line/adjoining stratiform (TL/AS), back-building/quasi-stationary (BB), broken line (BL), EL, and long line (LL) modes (Wang, Cui, et al., 2014). However, the general organizational features of MCSs in South China remain unknown.

Different organizational modes of MCSs correspond to different severe convective weather events due to different dynamic and thermodynamic processes (Bluestein & Jain, 1985; Duda & Gallus, 2010; Gallus et al., 2008; Lombardo & Colle, 2011; Parker, 2007; Parker & Johnson, 2000; Yang & Sun, 2018). Yang and Sun (2018) recognized six organizational modes over North China for severe wind-producing convective system events, consisting of cluster cells (35.4%), squall lines (18.4%), nonlinear-shaped systems (17.8%), broken lines (11.6%), individual cells (1.2%), and bow echoes (0.5%). Schumacher and Johnson (2005) found that TL/AS and BB were the two most frequent modes in 116 extreme rainfall events from 1999 to 2001 east of the Rocky Mountains in the United States, possibly due to their slow movements. For flooding events over the central United States that occurred during the period of April 1–August 31, 2002, Gallus et al. (2008) found that nonlinear systems were the dominant organizational mode among the nine predominant morphologies (including individual cells, clusters of cells, BL, BE, TS, LS, PS, NS, and NL) of all associated convective systems. However, studies on the general organization of MCSs associated with warm-sector heavy rainfall, which is characterized by severe intensity, rapid development, and localized distribution, have been quite limited.

The organizational aspect of warm-sector heavy rainfall in South China has been examined mainly using precipitation or satellite data. Based on hourly precipitation data, the characteristics of the synoptic situations and evolutions (including the orientation, extension, and motion) of warm-sector rainfall events in the coastal region of South China were investigated without distinguishing different organizational modes of the associated MCSs (Liang et al., 2019). By analyzing infrared satellite imagery during the presummer rainy season, Liang et al. (2012) demonstrated that a persistent elongated convective system (PECS) occurs most frequently among four types of MCSs according to the areas and eccentricities of cold cloud tops in South China. Nonetheless, unlike radar, neither satellite imagery nor precipitation data can provide detailed arrangement of convective and stratiform regions and thus has difficulty in distinguishing among different organizational modes. Recently, based on radar analyses for case studies, a mode of "band training" with multiple parallel back-building rain bands (MRBs) was found in warm-sector heavy rainfall events in South China (Liu et al., 2018; Wang, Luo, & Jou, 2014; Wu & Luo, 2016). However, no attempts have yet been made to analyze the statistical characteristics of the organizational modes of MCSs that are associated with warm-sector heavy rainfall in South China using radar data.

How the morphologies of MCSs are related to synoptic and mesoscale environments is also an interesting question and is important for operational forecasting practices. Wind fields have been shown to be key factors in distinguishing different organizational modes over the central United States and East China (Parker & Johnson, 2000; Wang, Cui, et al., 2014). The TS mode has significant rearward line-perpendicular storm-relative wind compared with other organizational modes. Relative to the general wind field, the vertical wind shear is a more critical factor affecting the morphology and evolution of an MCS. Zheng et al. (2013) examined the differences of linear MCS cases between dry and moist environments and showed that the BE mode over central East China generally occurs under the conditions of strong low-level wind shear and intermediate moisture. Thermodynamic variables may also have apparent differences among different organizational modes. Parker and Johnson (2000) proposed that the TS mode is associated with

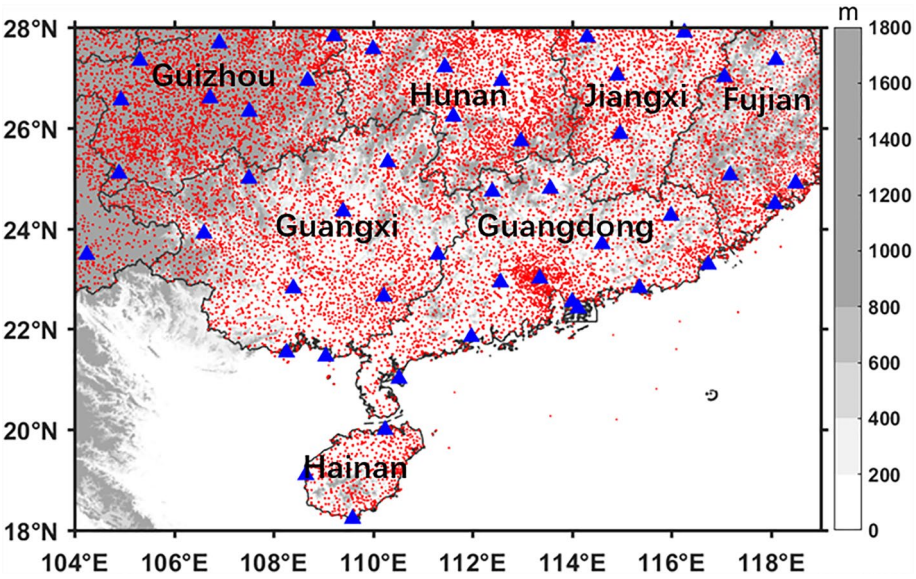

Figure 1. Distribution of radar stations (blue triangles) and rain gauges (red dots) in South China. The shading shows the terrain.

higher precipitable water, stronger surface cold pool temperature perturbation, and lower lifting condensation levels (LCLs) and convective condensation levels (CCLs) than those associated with the LS and PS modes over the central United States. However, the differences in environmental characteristics between different organizational modes of MCSs associated with warm-sector heavy rainfall in South China have not been analyzed.

This study aims to investigate the statistical characteristics of the organizational modes of MCSs associated with warm-sector heavy rainfall in South China based on composite radar reflectivity data during April–June from 2007 to 2020. The environmental characteristics of MCSs with different organizational modes were also examined. Section 2 describes the data and analysis methods. Section 3 presents the frequency and distribution characteristics of the different organizational modes of MCSs associated with warm-sector heavy rainfall in South China. Sections 4 and 5 examine the environmental and precipitation characteristics of the different organizational modes, respectively. Finally, a summary is given in Section 6.

2. Data and Methodology

2.1. Data

This study focuses on warm-sector heavy rainfall events during April–June from 2007 to 2020 in South China, covering Guangdong Province, Guangxi Province, Hainan Province, and the southern regions of Fujian, Jiangxi, Hunan, and Guizhou Provinces, from approximately 18°–28°N and 104°–119°E. The regional radar mosaic of composite reflectivities that was used to investigate the initiations, formations, evolutions, and dissipations of convective systems was provided by the National Meteorological Center (NMC) of the China Meteorological Administration (CMA). The Doppler radar network in China was constructed in 1998 and had 112 operational radars as of 2007 and 205 operational radars in 2020. The composite reflectivities have a spatial resolution of 2 km and a temporal resolution of 20 min in 2007–2008, 10 min in 2009–2016, and 6 min since 2017, contoured from 10 to 70+ dBZ with an increment of 5 dBZ. There are 47 radar stations in the target region with an integrity rate of 95.4%. The environmental parameters of the different organizational modes were analyzed using the hourly European Center for Medium-Range Weather Forecasts (ECMWF) ERA5 reanalysis data set (Hersbach et al., 2018a, 2018b), with a resolution of 0.25° × 0.25°. Hourly rainfall observation from rain gauges, which were provided by the CMA (totaling 16,140 stations; locations given in Figure 1), were used to analyze the precipitation features of the different organizational modes.

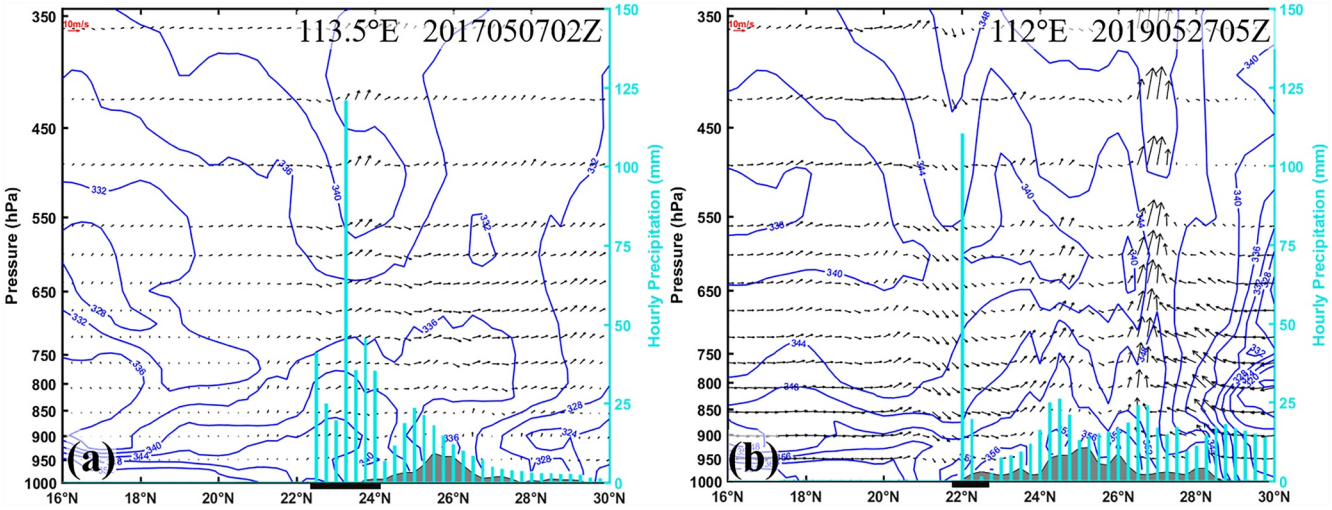

Figure 2. Meridional-vertical cross sections of two warm-sector heavy rainfall events: (a) without a surface front at 02 Z on May 7, 2017; (b) ahead of a frontal system at 05 Z on May 27, 2019. The blue line represents the potential pseudoequivalent temperature (θ_{se}, units: K), and the cyan bars indicate the 6-h cumulative precipitation values (mm). The arrow is the wind vector (m s^{-1}), and the gray shading is the terrain. The heavy black line on *x*-axis denotes the location of warm-sector heavy rainfall.

2.2. Identification of MCSs Associated With Warm-Sector Heavy Rainfall

Each MCS that was associated with warm-sector heavy rainfall was identified using the following five criteria: (a) a reflectivity of ≥40 dBZ lasts at least 3 h with a reflectivity of 30 dBZ having a length scale of ≥ 100 km for at least 3 h; (b) the MCS produces at least 20-mm maximum hourly rainfall; (c) the MCS occurs without an associated frontal system (e.g., Figure 2a) in South China and produces rainfall at least 200 km ahead of the surface northerly wind ($v < 0$) or at least 200 km ahead of a frontal system (e.g., Figure 2b); (d) when a warm-sector heavy-rainfall-associated MCS and a frontal-rainfall-associated MCS occur simultaneously in South China, the warm-sector heavy-rainfall-associated MCS is at least 200 km away from the frontal-rainfall-associated MCS, and there is no merging of these two types of MCSs during the whole lifespan; (e) the identified MCS is not associated with a tropical depression or tropical cyclone. The frontal system is precisely identified as the dense region of potential pseudoequivalent temperature (θ_{se}), which is widely used to determine the position of a front (e.g., Chen et al., 2012; Ding et al., 2011; Liu et al., 2019).

The lifespan of an MCS is defined as the period when the MCS threshold is continuously met. The time of the convection initiation (CI) of each MCS is determined when the radar reflectivity value first reaches 35 dBZ. Convective precipitation is defined when the reflectivity value is no less than 40 dBZ, while stratiform precipitation is defined when the reflectivity value is between 20 and 40 dBZ (Parker & Johnson, 2000). The "convective line" in the definition of the organizational modes in the following section means the linear convective precipitation part (≥40 dBZ) of each MCS.

2.3. Classification of Organizational Modes of MCSs

We classified the morphologies of MCSs according to the arrangement of the convective and stratiform precipitation regions as well as the morphologies of the regions of convective reflectivities, following the definitions of different organizational modes outlined by Parker and Johnson (2000), Schumacher and Johnson (2005), Wang, Luo, and Jou (2014), and Zheng et al. (2013). The morphology of an MCS may change during its lifespan. We are interested in the dominant organizational mode that effectively produces heavy rainfall in the identified MCS cases. An organizational mode is assigned to an MCS case at the maturation time, which is defined as the time when the area of reflectivity of ≥45 dBZ is the largest during the lifespan of the MCS. Because our target systems are MCSs with the reflectivity of 30 dBZ having a length scale of ≥ 100 km, cellular types are not included. The organizational modes of the 92 total MCSs were classified into nine categories, including the NL mode and eight linear modes, including NS, EL, TS, BE, LS, PS, TL/AS, and MRB. The definitions of TS, LS, and PS modes mainly follow Parker and Johnson (2000). The definitions

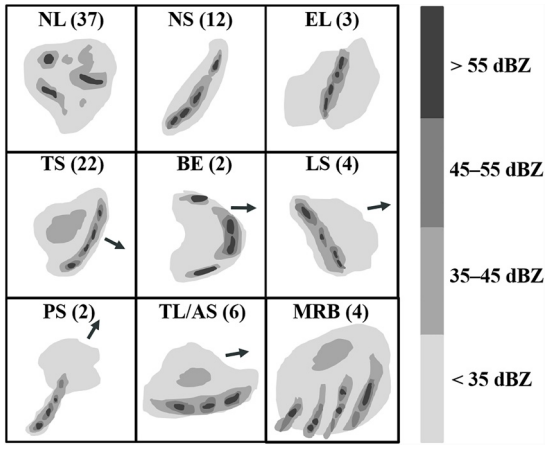

Figure 3. Schematic reflectivities illustrating the morphologies of the nine organizational modes. This classification of mesoscale convective systems (MCSs) considers the arrangement of convective and stratiform regions, the morphology of convective reflectivities and the direction of the motion of the convective system. The arrow indicates the direction of the movement of the MCS. The numbers in parentheses indicate the number of samples of the corresponding organizational mode that occurred during the examined period.

of NS, PS, BE, and EL modes mainly follow Zheng et al. (2013), while the definitions of TL/AS and MRB modes mainly follow Schumacher and Johnson (2005) and Wang, Luo, and Jou (2014), and Wang, Cui, et al. (2014), respectively. We defined the organizational modes in a more quantitative way so that each mode can be clearly and objectively distinguished from others. Schematic morphologies of the reflectivities of different organizational modes are shown in Figure 3, with typical real-case examples shown in Figure 4.

An MCS is defined to have a linear mode if the radar reflectivity of ≥40 dBZ has a length-to-width ratio of at least 1.8. Otherwise, it is classified as an NL mode. Linear modes are further classified into the following eight organizational modes.

2.3.1. NS: No Stratiform Precipitation

A convective line consisting of continuous or quasi-continuous convective cells is defined as NS when a strong reflectivity gradient is observed at both the leading and trailing edges (the maximum widths of the preline and postline stratiform precipitation are less than the maximum width of the convective line). Other linear modes are distinguished from the NS mode by having the maximum width of the preline or postline stratiform precipitation greater than the maximum width of the convective line.

2.3.2. EL: Embedded Lines

At least two-thirds of the convective line is embedded in a large area of stratiform precipitation. The maximum widths of the preline and postline stratiform precipitation are both larger than the maximum width of the convective line. The following linear modes, which have stratiform precipitation, occur with the fashion of nonembedded lines.

2.3.3. TS: Trailing Stratiform Precipitation

Stratiform precipitation is dominantly located behind the convective line with respect to the direction of the movement of the MCS and moves generally perpendicularly to the convective line. The maximum width of the trailing stratiform precipitation is larger than the maximum width of the convective line. There is usually a great reflectivity gradient at the leading edge of the MCS. The distance from the apex of the leading edge to the straight line connecting the two ends of the convective line is smaller than half the total distance of the straight line from end to end, which is used to distinguish it from the bow echoes mode.

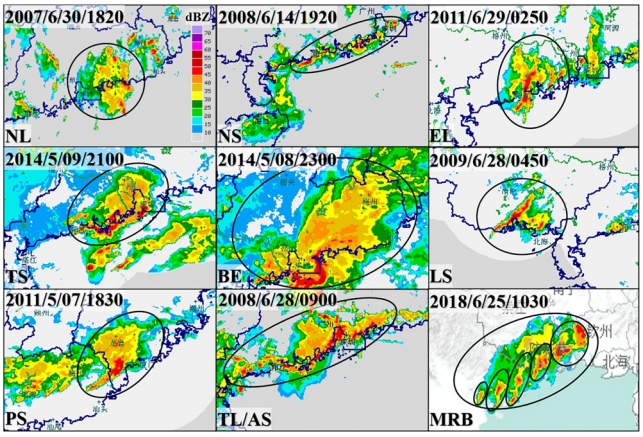

Figure 4. Nine typical organizational modes of mesoscale convective systems (MCSs; in black ellipse) observed in radar images. Multiple parallel rainbands have been marked by the smaller black ellipses in the multiple rain bands (MRB) case.

2.3.4. BE: Bow Echoes

Similar to the TS mode, but with the distance from the apex of the leading edge to the straight line connecting the two ends of the convective line being at least half the total distance of the straight line from end to end. The convective reflectivities have the shape of a bow or crescent and a great gradient exists at the convex region. The BE mode is closely related to severe winds and tornadoes (Weisman, 2001).

2.3.5. LS: Leading Stratiform Precipitation

Similar to the TS mode, except stratiform precipitation is dominantly located in advance of the convective line with respect to the direction of the movement of the MCS. A great reflectivity gradient exists at the trailing edge of the MCS.

2.3.6. PS: Parallel Stratiform Precipitation

The convective line has at most one-third of its length embedded in the downstream stratiform precipitation that moves roughly parallel to the

orientation of the convective line (generally less than 30° from the orientation of the convective line) with a maximum width larger than the maximum width of the convective line. The other at least two-thirds of the convective line has a strong reflectivity gradient at both the leading and trailing edges.

2.3.7. TL/AS: Training Line/Adjoining Stratiform

The convective line has at least two-thirds of its length adjoining with stratiform usually on the north side, with a maximum width larger than the maximum width of the convective line. Both stratiform and convective precipitation move along the orientation of the convective line.

2.3.8. MRB: Multiple Rain Bands

There are at least four approximately parallel convective lines with at least one convective line having a length of ≥100 km. These convective lines are partly or completely embedded in stratiform precipitation.

2.4. Calculation Method of Environmental Parameters

The environmental parameters of the organizational modes were analyzed using ERA5 data immediately prior to the initiation of the target MCS, including vertical wind shear, relative humidity, most unstable convective available potential energy (MUCAPE), most unstable convective inhibition (MUCIN), lifted index (LI), Total Totals index (TTI), K index, and precipitable water. Vertical wind shear is determined by the magnitude of the vector difference between the wind at the desired altitude (e.g., 1, 3, or 6 km) and the wind at a height of 10 m above the ground. The MUCAPE and MUCIN were calculated using the parcel of air that gives the greatest absolute values of convective available potential energy and convective inhibition, respectively, among the parcels departing at different levels from the ground to 350 hPa. The TTI is the sum of the difference between 850-hPa temperature ($T_{850\text{hPa}}$) and 500-hPa temperature ($T_{500\text{hPa}}$) and the difference between 850-hPa dewpoint ($Td_{850\text{hPa}}$) and 500-hPa temperature as a measure of the moisture content between 850 and 500 hPa, and can be expressed as

$$\text{TTI} = \left(T_{850\text{hPa}} - T_{500\text{hPa}}\right) + \left(Td_{850\text{hPa}} - T_{500\text{hPa}}\right)$$

The LI is the difference between the environmental temperature at 500 hPa and the air parcel temperature at 500 hPa that is lifted from the ground. A nonparametric test, the Kruskal-Wallis test (Kruskal & Wallis, 1952), was used to test whether the medians of the environmental parameters among the top three organizational modes have significant differences. The significant difference in parameters between any two modes was tested using the Wilcoxon rank sum test (Wilcoxon, 1945).

2.5. Calculation Method of Average Maximum Rainfall

Based on hourly precipitation produced by the convective systems we focused on, the maximum 1-, 3-, and 6-h accumulated precipitation values associated with the assigned organizational mode of each system were identified. First, the influence area of the target system is determined by the maximum and minimum values of longitudes and latitudes where the system covers in composite radar images during its lifespan. Then, all the rainfall gauges in the influence area are located and the hourly precipitation produced by other systems are removed to form a record base to produce the maximum precipitation of different thresholds. The maximum 1-h (3- or 6-h) precipitation records are then selected during the period from 1 h (3 or 6 h) immediately before the beginning of the assigned organizational mode to 1 h (3 or 6 h) after the morphology of the MCS no longer meets the definition of the corresponding organizational modes. Finally, the maximum 1-h (3- or 6-h) precipitation records of all systems of each mode are averaged.

Table 1
Dates of the Initiation Time of Convective Systems Associated With Warm-Sector Heavy Rainfall Events in South China

NL (37)	27 Jun 2007 (2)	7 Jun 2009	7 Jun 2010	7 May 2011 (2)	11 Jun 2011
	15 Jun 2011 (2)	28 Jun 2011	8 May 2013	22 May 2014	1 Apr 2015
	15 May 2015	19 Apr 2016	13 Jun 2016	6 May 2017	14 Jun 2017
	21 Jun 2017 (2)	22 Jun 2017	29 Jun 2017	13 Apr 2018	20 Apr 2018
	29 Apr 2018	2 May 2018	10 May 2018	20 Jun 2018	22 Jun 2018
	23 Jun 2018	24 May 2019 (2)	26 May 2019	27 May 2019	19 May 2020
	24 May 2020	15 Jun 2020	–	–	–
NS (12)	27 Jun 2007	13 Jun 2008	14 Jun 2008	28 Jun 2008	8 May 2013
	18 May 2015	9 Jun 2016	14 Jun 2017	25 May 2019	17 Jun 2019
	25 Jun 2019	17 Jun 2020	–	–	–
EL (3)	28 Jun 2011	7 May 2013	29 May 2019	–	–
TS (22)	26 Jun 2007	28 Jun 2007	30 Jun 2007	27 Jun 2008 (2)	8 Jun 2009
	27 Jun 2009	9 May 2014	3 Apr 2016	21 Apr 2016	21 Jun 2018 (2)
	18 Apr 2019	19 Apr 2019	4 Jun 2019	5 Jun 2019	11 Jun 2019 (2)
	14 Jun 2019	16 Jun 2019	5 Jun 2020	10 Jun 2020	–
BE (2)	27 Jun 2011	8 May 2014	–	–	–
LS (4)	27 Jun 2009	8 May 2016	6 May 2017	20 Apr 2019	
PS (2)	6 May 2011	21 Jun 2017	–	–	–
TL/AS (6)	27 Jun 2008	22 Jun 2018	23 Jun 2018	17 Apr 2019	29 May 2020
	14 Jun 2020	–	–	–	–
MRB (4)	24 Jun 2018 (2)	26 May 2019	8 Jun 2020	–	–

Note. The numbers in parentheses in the first column indicate the numbers of all MCSs with the corresponding modes, and the other numbers in parentheses indicate the number of MCSs that occurred on the corresponding days. Cases with the same indicated times occurred in different regions.

BE, bow echoes; EL, embedded lines; LS, leading stratiform precipitation; MCSs, mesoscale convective systems; MRB, multiple rain bands; NS, no stratiform precipitation; NL, nonlinear mode; PS, parallel stratiform precipitation; TS, trailing stratiform precipitation; TL/AS, training line/adjoining stratiform.

3. The Frequency and Distribution of Different Organizational Modes

3.1. Frequency

A total of 92 MCSs associated with warm-sector rainfall in South China were identified during April–June from 2007 to 2020 using the criteria described in Section 2.2 (Table 1), in which 40% are representative of the NL mode and 60% are representative of linear organizational modes (Figure 5a). The TS mode is the most frequent among all linear modes, accounting for 40% of the total linear modes (Figure 5b). The second most frequent linear mode is the NS mode, which accounts for 22% of the total linear modes. The TL/AS mode accounts for 11% of the total linear modes, ranking third among all linear modes. The MRB and LS modes individually account for 7% each of the total linear modes. The EL mode accounts for 5% of the total linear modes. The PS and BE modes are quite rare in warm-sector rainfall-associated MCSs in South China and individually account for only 4% each of the total linear modes.

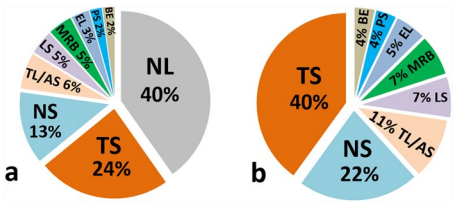

Figure 5. Percentage of (a) each morphology among the 92 morphological samples and (b) each linear morphology among the 55 linear morphological samples.

Among all nine individual modes, the NL mode is the most frequent, which is similar to what was observed in flooding events over the central United States (Gallus et al., 2008). The top two most frequently observed organizational modes (40% for NL and 24% for TS) are the same as the statistical results over the Yangtze River basin but with different percentages (48.5% for NL and 11.6% for TS; Wang, Cui, et al., 2014). Over central East China, the most frequent mode is also the NL, however, the EL

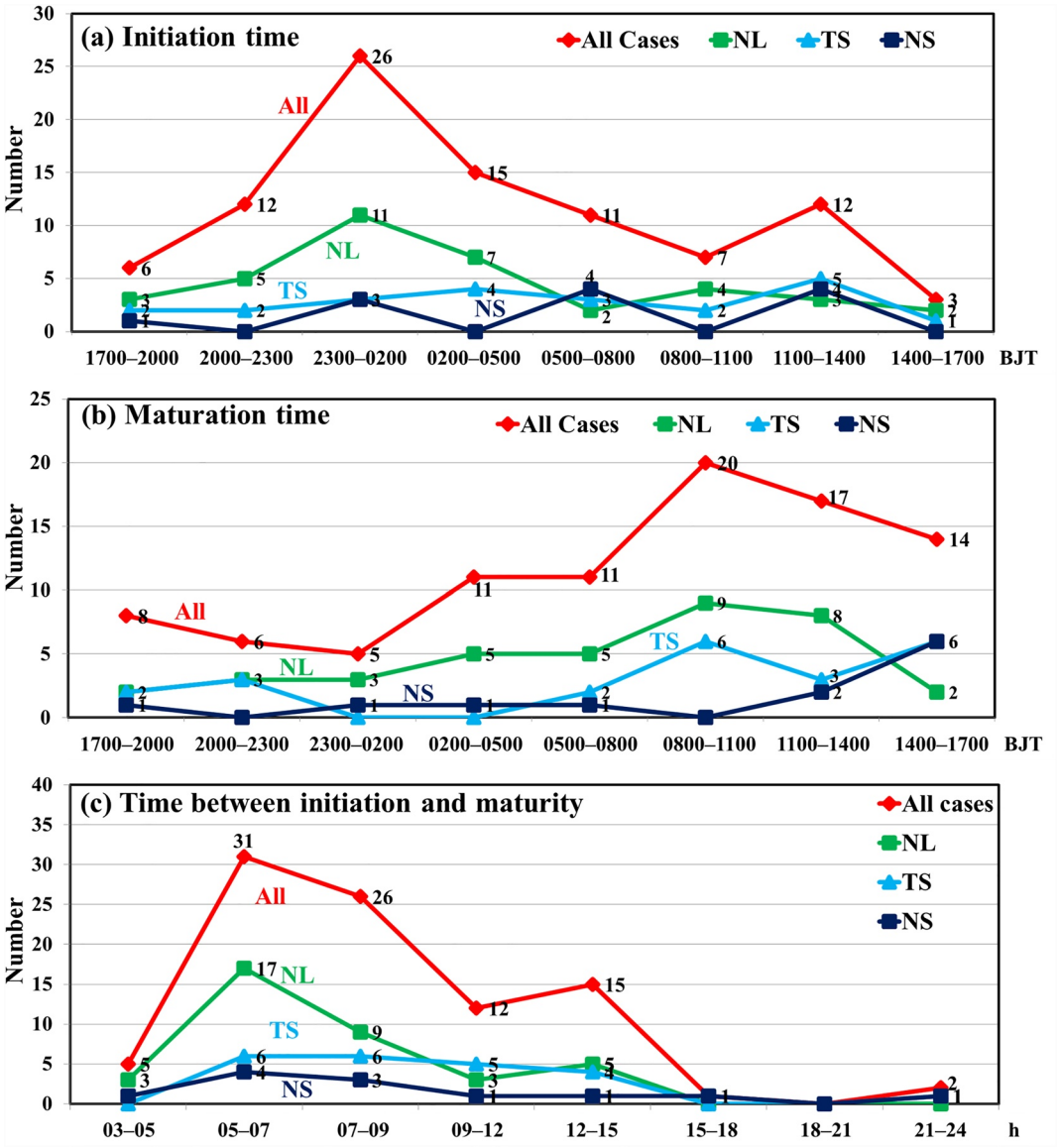

Figure 6. Distributions of the initiation time (a), maturation time (b), and time between initiation and maturity (c) for all cases and the top three most frequent organizational modes. Time is BJT (BJT = UTC + 8 h).

mode is the most prevalent linear mode, with a proportion of 22.7% of all linear modes, slightly higher than those of the NS (21.6%) and TS (19.3%) modes (Zheng et al., 2013). We mainly focus on the top three most frequently observed organizational modes (NL, TS, and NS) of MCSs which account for 77% of all target MCSs in the following discussion.

3.2. Temporal Distribution

The diurnal distribution of the initiation times of the MCSs associated with warm-sector heavy rainfall displays double peaks (Figure 6a). The major peak is in the early morning (2300–0200 BJT, BJT = UTC + 8 h) and accounts for 28% of the total, different from the predominant initiation time peak observed in the afternoon over the Yangtze River basin (Wang, Cui, et al., 2014). The minor peak observed in this study occurs in the early afternoon (1100–1400 BJT) and accounts for 13%. The MCSs in the period of early morning peak mainly initiate in the coastal area (Figure 7c) and can be explained by the convergence between land breezes in the early morning and southwesterly airflows during the presummer rainy season, while the early

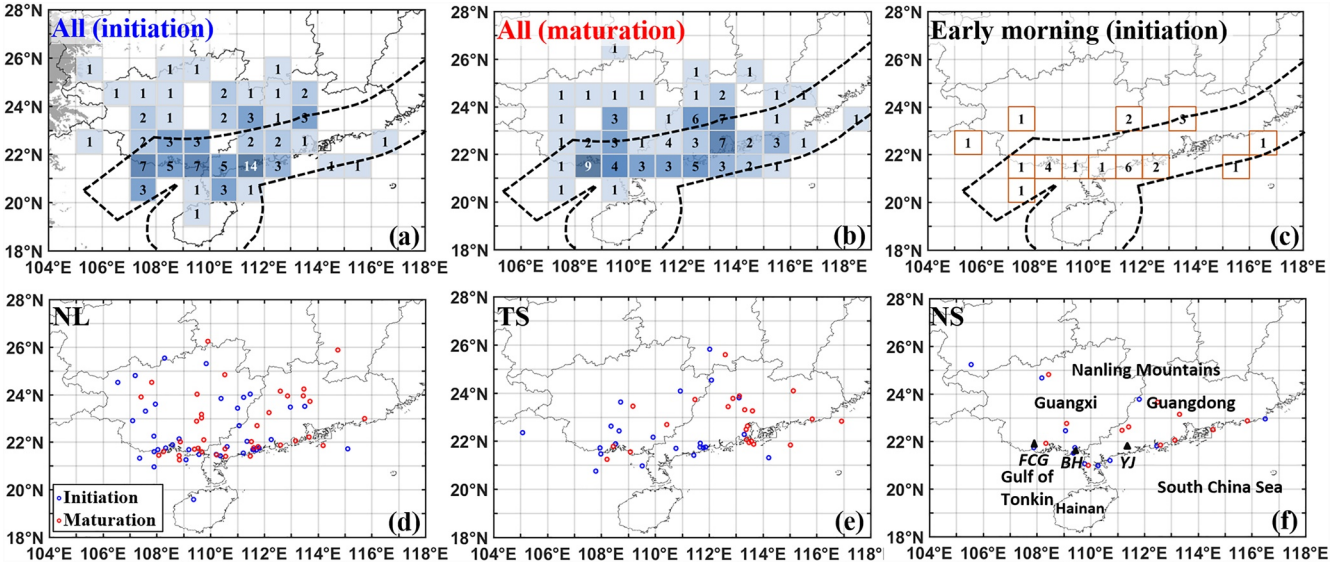

Figure 7. The locations of initiation (a) and maturation (b) for all mesoscale convective systems (MCSs), and initiation of MCSs which occur in the early morning 2300–0200 BJT, (c). The terrain higher than 1,500 m above sea level in South China is given in shading in (a) for reference. The dash lines in (a–c) indicate the coastal region, approximately 100 km away from the coastline. The number in each grid in (a–c) indicates the number of times that the initiation (maturation) locations of the MCSs appear in that grid. The initiation (blue circle) and maturation (red circle) locations for the top three most frequent organizational modes are shown in (d–f). The black triangles in (f) represent Fangchenggang city (FCG), Beihai city (BH), and Yangjiang city (YJ).

afternoon peak has been explained by low-level atmospheric instability resulting from surface solar heating in the afternoon (e.g., Dai et al., 1999; Yu et al., 2007; Zhou et al., 2008). The major peak in the early morning is mainly contributed to by MCSs of the dominant NL mode, which has an early morning peak (accounting for 30% of NL modes) similar to the features of all modes combined. The initiation times of the TS and NS modes are generally evenly spread throughout the day without showing an apparent peak.

The diurnal distribution of the maturation times of warm-sector rainfall-associated MCSs shows an obvious peak at 0800–1100 BJT, approximately 9 h after the major initiation time peak (Figures 6a and 6b), which accounts for 22% of the total. The maturation time of each MCS is defined as the time when the area of reflectivity of ≥45 dBZ is the largest during the lifespan of the MCS. Similar to the initiation times, the peak of the maturation times of the NL mode is the same as the maturation time peak of all MCSs. The NS mode has a significant maturation time peak in the afternoon (1400–1700 BJT), with a proportion of 50% at the maturation time peak. The maturation times of TS modes have no apparent major peak in the diurnal distribution. The maturation time of most MCSs is 5–15 h after their initiation times (Figure 6c). MCSs of the NL mode take significantly shorter time to reach maturity than do the linear modes (based on Wilcoxon rank sum test). Forty-six percent of NL modes have durations of 5–7 h from initiation to maturity. The proportion of MCSs of the NL mode among all MCSs decreases as the time between initiation and maturity increases. MCSs with 9–15 h between initiation and maturity mainly consist of linear modes. A few systems of linear modes even take more than 20 h to reach maturity. The short duration between initiation and maturation of the NL mode systems could be related to the more humid environment associated with this mode, as demonstrated in Section 4.

The average lifespan of all MCSs associated with warm-sector heavy rainfall in South China is 11.0 h, which is consistent with the statistical results based on hourly precipitation data in which the average lifespan of warm-sector heavy rainfall events was 11.58 h (Liu et al., 2019). MCSs of linear modes tend to last significantly longer than those of the NL mode (based on Wilcoxon rank sum test), agreeing with the statistical results obtained over central East China (Zheng et al., 2013). The average lifespan of the NL mode is 8.8 h (Table 2), which is shorter than the average lifespan of any individual linear mode and the average lifespan (12.5 h) of all linear modes combined. The average lifespans of the linear modes become longer from the NS (9.5 h) to the MRB (9.9 h), LS (10.5 h), TS (12.2 h), PS (12.2 h), TL/AS (15.5 h), EL (15.8 h), and BE (28.1 h) modes. The longest lifespan is 35 h, which was observed in a BE case.

Table 2
Average Lifespans of Different Organizational Modes

Mode	NL	Linear	TS	NS	MRB	LS	PS	TL/AS	EL	BE
Lifespan (h)	8.8	12.5	12.2	9.5	9.9	10.5	12.2	15.5	15.8	28.1

Note. BE, bow echoes; EL, embedded lines; LS, leading stratiform precipitation; MRB, multiple rain bands; NS, no stratiform precipitation; NL, nonlinear mode; PS, parallel stratiform precipitation; TS, trailing stratiform precipitation; TL/AS, training line/adjoining stratiform.

The majority of the warm-sector rainfall-associated MCSs occur in June (60%), with only 28% of MCSs occurring in May and 12% occurring in April (Table 3), which is consistent with the monthly distributional features observed for warm-sector heavy rainfall during the rainy season (Liu et al., 2019). Linear modes account for 55% of all MCSs in April, 46% of all MCSs in May, and increase to 67% in June. During the presummer rainy season, relative to those in April and May, all the top three most frequent organizational modes have the highest occurrences in June (49% of the NL mode, 77% of the TS mode, and 75% of the NS mode) when the prevailing southwesterly monsoon provides favorable warm and moist airflows.

3.3. Geographical Distribution

The initiation locations of all MCSs are mainly distributed in the area with the terrain height below 1,500 m above sea level along the coastlines of Guangdong and Guangxi Provinces (Figure 7a), with the major concentrated center located in Yangjiang city (111°–112°E, 21°–22°N; the location is given by a black triangle denoted by "YJ" in Figure 7f), which may be related to the enhanced convergence produced by the collision of low-level southwesterly or southerly winds with coastal mountains approximately parallel to the coastline and their associated land breezes (Bai et al., 2020; Liang et al., 2019). Minor concentrated centers are located in Fangchenggang and Beihai cities (locations are given by black triangles denoted by "FCG" and "BH" in Figure 7f). The initiation (maturation) location is defined as the centroid point of the strongest reflectivity at the initiation (maturation) time. Most NL systems initiate near the coastline of south Guangxi and west Guangdong Provinces (Figure 7d). Sixty-three percent of TS systems initiate in Guangdong and Guangxi Provinces along the coastlines, especially 23% of TS systems initiate in Yangjiang city (Figure 7e). Seventy-five percent of NS systems initiate near the coastlines of Guangdong and Guangxi Provinces (Figure 7f).

The spatial distribution of the maturation locations of all MCSs displays two concentrated centers (Figure 7b). One center is slightly east of the minor initiation concentrated center in Fangchenggang city. The other center is located in the Pearl River Delta, obviously east of the major initiation concentrated center, which is located on the southern plain of the Nanling Mountains (the location is given in Figure 7f). The maturation locations of NL systems are quite close to their initiation locations (Figure 7d), while the maturation locations of the linear systems are obviously east of their initiation locations (especially for those of the TS mode). This result is possibly contributed to partly by the shorter lifespans and slower movements of systems of the NL mode than those of systems of the two linear modes. The slower movements of systems of the NL mode are confirmed by the statistics on their movements. NL systems account for 53% of MCSs with quasi-static movement. A quasi-static MCS is defined as an MCS whose geometric center of reflectivity of ≥40 dBZ moves not exceeding 30 km within three consecutive hours around its maturation time. This criteria of 30 km per 3 h is about one fifth of the mean distance of squall lines in East China (Meng et al., 2013).

Table 3
Monthly Distributions of Different Organizational Modes

Mode	All	NL	Linear	TS	NS	EL	BE	PS	LS	TL/AS	MRB
April	11	5	6	4	0	0	0	0	1	1	0
May	26	14	12	1	3	2	1	1	2	1	1
June	55	18	37	17	9	1	1	1	1	4	3

Note. BE, bow echoes; EL, embedded lines; LS, leading stratiform precipitation; MRB, multiple rain bands; NS, no stratiform precipitation; NL, nonlinear mode; PS, parallel stratiform precipitation; TS, trailing stratiform precipitation; TL/AS, training line/adjoining stratiform.

Forty-nine percent of MCSs associated with warm-sector heavy rainfall move northeastward in terms of the direction of the movement of the dominant organizational mode at the maturation time (Figure 8). The northeastward movement of the MCSs is related to southwesterly low-level jets (LLJs) and the southwesterly mean cloud-layer winds generally in front of a westerly trough and west of the subtropical high. Both the NL and TS modes have northeastward movements as the highest-frequency

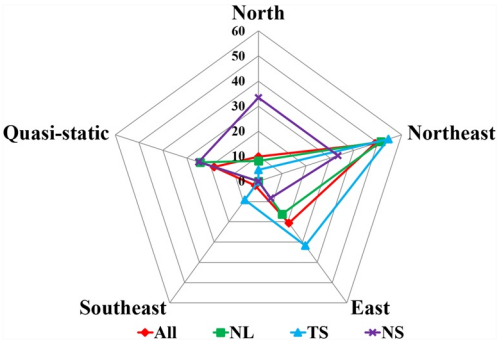

Figure 8. Percentages of the directions of movement of all mesoscale convective systems (MCSs) and those of the top three most frequent organizational modes.

movement direction. Among the top three organizational modes, the TS mode has the highest proportion of movements in the northeast direction, with 32% of TS systems moving east and fewer than 10% individually moving either north or southeast. Of all NS systems, 33%, 33%, and 25% move north, northeast, and stay quasi-static, respectively.

3.4. Formation Mode

MCSs associated with warm-sector heavy rainfall with different organizational modes have different formation modes. Classical formation modes of squall lines were proposed by Bluestein and Jain (1985) based on cases in Oklahoma in the United States, including broken line, back building, broken areal, and embedded areal formation modes. Some of these formation modes were also listed as organizational modes in some recent works (e.g., Gallus et al., 2008; Schumacher & Johnson, 2005; Yang & Sun, 2018). Referring to the classification method of Bluestein and Jain (1985), we examined the formation modes of general MCSs associated with warm-sector heavy rainfall in South China rather than just those of linear MCSs, as shown in Figure 9. Typical real-case formation processes of MCSs observed in radar images are shown in Figure 10. The broken line mode is defined as discrete convective cells arranging in a line and merging into a linear convective system. The back building mode refers to new cells repeatedly appearing in the upstream and merging with old cells. The formation mode in which the convective system forms by the merging of scattered cells is termed the broken areal. The embedded areal mode is defined as the formation mode in which discrete convective cells form within a stratiform region. If several formation modes are involved in the formation process of an MCS, the predominant formation mode is assigned.

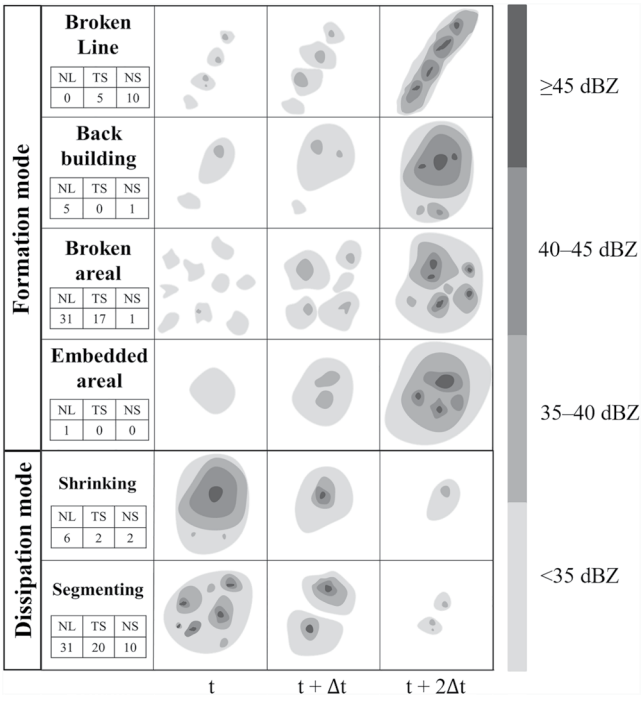

Figure 9. Schematic diagram of the formation processes and dissipation processes of the mesoscale convective systems (MCSs) associated with warm-sector heavy rainfall events in South China. The frequencies of the formation modes and dissipation modes of the top three most frequent organizational modes are shown in the second column.

The results show that the broken areal mode is the most predominant formation mode of MCSs associated with warm-sector heavy rainfall in South China. Eighty-four percent of NL and 77% of TS systems form via the broken areal mode (Figure 9). A total of 83% of NS systems form via the broken line mode. The dominance of the broken areal formation mode could be related to the moist environment in South China associated with the southwest monsoon, which possibly favors the occurrences of amorphous convections (Schumacher & Peters, 2017).

3.5. Dissipation Mode

In addition to the formation modes, the dissipation modes of the top three most frequent organizational modes were also examined in this study. Meng et al. (2013) proposed three main dissipation modes for squall lines in East China: the reversed broken line, shrinking line and reversed broken areal modes. The dissipation modes of general MCSs rather than those of just squall lines have rarely been examined thus far in the literature. The dissipation modes of the MCSs examined in this work were classified as shrinking and segmenting, as shown in Figure 9 with typical real-case examples shown in Figure 10. The contiguous shrinkage of the zone of reflectivity of ≥35 dBZ in a convective system is termed the shrinking mode. In the segmenting mode, the convective system breaks into a few segments, and each segment gradually dissipates. Using this classification method, we found that the segmenting mode accounts for 84% of the dissipation modes of the total MCSs associated with warm-sector heavy rainfall in South China. Eighty-four percent of NL systems dissipate via the segmenting mode, and 16% dissipate via the shrinking mode. Ninety-one percent of TS systems and 83% of NS systems dissipate via the segmenting mode.

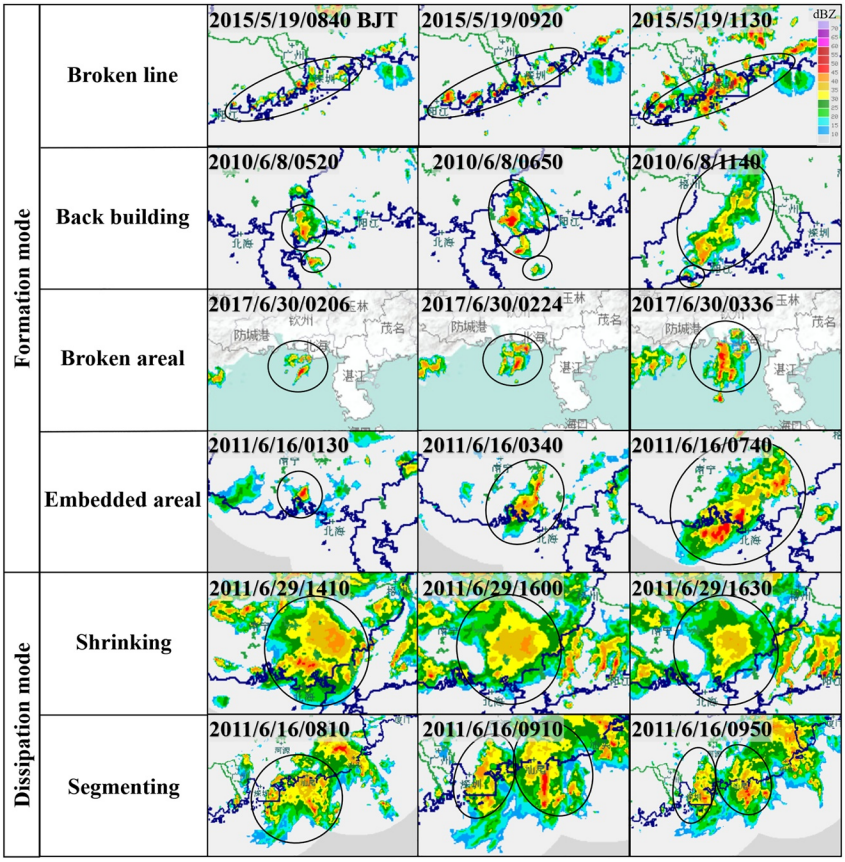

Figure 10. Typical formation and dissipation modes of mesoscale convective systems (MCSs; in black ellipse) observed in radar images.

3.6. Features of Organizational Modes With Relatively Low Frequency

Organizational modes of MCSs with relatively low frequency, including the TL/AS, MRB, LS, EL, BE, and PS modes, are categorized as other organizational modes, and their general temporal and geographical distributions, movement features, formation and dissipation processes are briefly summarized here. Other organizational modes of MCSs have the same early morning peak at 2300–0200 BJT (43%) in their initiation times as all the top three most frequent organizational modes combined (NL, TS, and NS modes), but rarely occur in the afternoon (1100–1700 BJT) which is different from the early afternoon peak (1100–1400 BJT) in the initiation times of all the top three modes combined. The maturation times of MCSs of other organizational modes evenly spread throughout the day without showing an apparent peak, which is different from the double peaks of maturation times of all the top three modes combined at 0800–1100 BJT and 1400–1700 BJT. The average lifespan of other organizational modes of MCSs is 14.4 h, which is longer than that of all the top three modes combined because there are more long-lived linear modes in the other organizational modes.

Other organizational modes of MCSs have similar features as high-frequency modes in geographical distributions, movement, formation and dissipation. The majority of initiation and maturation locations are along the coastlines of Guangdong and Guangxi Provinces. Similar to most NL and TS modes having northeastward movements, half of other modes of MCSs move northeast, and 24% of other modes of MCSs move east or quasi-static. Four of five MCSs of other modes with quasi-static movement are the MRB mode, which is consistent with the high probability of the MRB mode in producing heavy rainfall. Most other modes of MCSs form via the broken areal mode, with only 24% form via the broken line mode and 19% via the back building mode. Other modes of MCSs dissipate via two dissipation modes with the same proportions as all the top three modes combined, with 86% via the segmenting mode and only 14% via the shrinking mode.

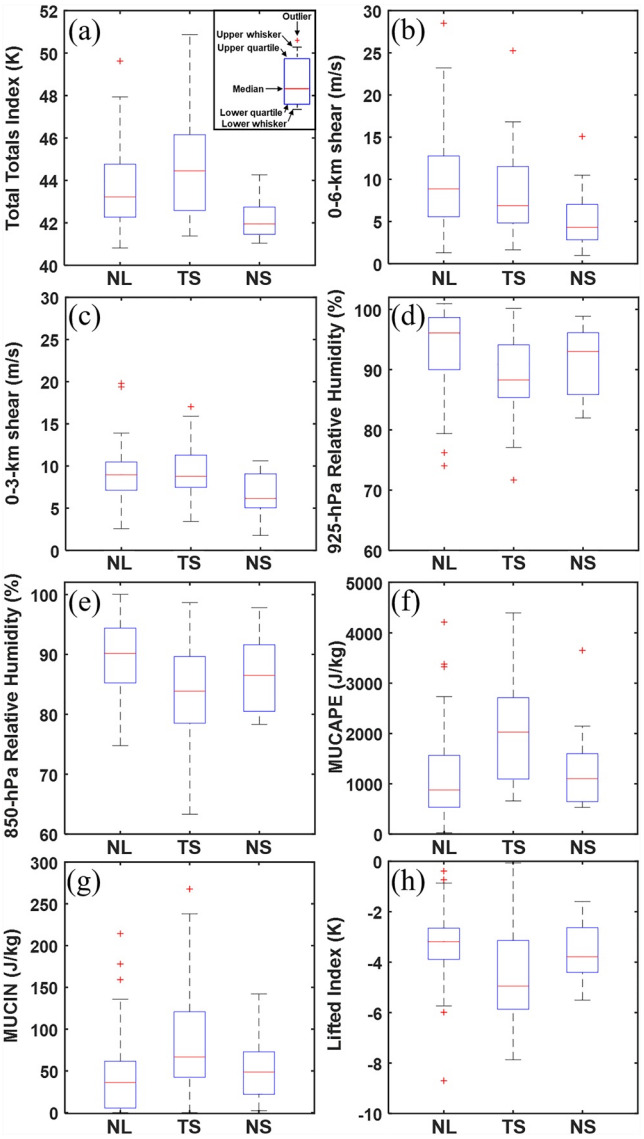

Figure 11. Box-and-whisker plots showing the Total Totals index (TTI) (a), 0–6-km shear (b), 0–3-km shear (c), 925-hPa relative humidity (d), 850-hPa relative humidity (e), most unstable convective available potential energy (MUCAPE) (f), most unstable convective inhibition (MUCIN) (g), and lifted index (h) values of the top three organizational modes. As shown in the legend of panel (a), the boxes denote the 25th (referred to as Q1 hereafter) to 75th (referred to as Q3 hereafter) percentiles. The short red lines in the boxes denote the median values, and the "+" symbols indicate outliers beyond the whiskers. The whiskers denote the extreme values of Q1 − 1.5 (Q3 − Q1) and Q3 + 1.5 (Q3 − Q1).

4. Environmental Characteristics for the Top Three Organizational Modes

4.1. Environmental Parameters

Our results show that the TTI is a great forecast factor for differentiating the top three organizational modes, with significant differences at the 99% significance level among all three modes. The TS mode occurs with the highest TTI, and the NS mode has the lowest TTI (Figure 11a). The NL mode has a significantly higher TTI than that of the NS mode at the 98% significance level and a significantly lower TTI than that of the TS mode at the 92% significance level.

The results also show that the 0–6- and 0–3-km wind shear in the NS mode are significantly smaller than those in the NL and TS modes (Figures 11b and 11c), with significantly different median values of 0–6-km (or 0–3-km) wind shear at the 98% (92%) significance level. However, the 0–6-km (or 0–3-km) wind shear of the NL and TS modes have no significant differences. The average 0–6-km wind shear of all organizational modes of MCSs associated with warm-sector heavy rainfall is approximately 8.8 m s^{-1}, which is much smaller than that observed over central East China, where the 0–6-km wind shear of all MCSs was found to be approximately 24 m s^{-1} (Zheng et al., 2013). The differences in the 0–1-km wind shear or deeper-layer wind shear (such as 0–10-km) among all the top three most frequent modes are not statistically significant.

Relative humidity at 925 and 850 hPa are also key factors in differentiating organizational modes. The NL mode has significantly higher 925- and 850-hPa relative humidity values than those of the TS mode at the 95% significance level (Figures 11d and 11e). The 850- and 925-hPa relative humidity values of the NS mode are not significantly different from those of the NL and TS modes. There are no significant differences in the higher-level (700 and 500 hPa) relative humidity values among the top three organizational modes. This conclusion is consistent with the results of numerical experiments showing that an increase in water vapor at the lower layer may favor the generation of less organized convection (Schumacher & Peters, 2017; Sun et al., 2014).

Additionally, the TS mode has significantly higher MUCAPE and MUCIN values and absolute values of LI than those of the other two organizational modes at the 90% significance level (Figures 11f–11h). The K index and precipitable water were also analyzed in this study; however, these factors do not show significant differences among the top three most frequent organizational modes.

4.2. Vertical Profiles of Prestorm Storm-Relative Wind

The prestorm storm-relative vertical wind profiles were examined in the top three organizational modes by calculating the prestorm line-parallel and line-perpendicular storm-relative winds at 925, 850, 700, 500, and 200 hPa. The orientation of the line of each MCS is defined as the orientation of the tangent line of the strongest echo in the convective line of the TS and NS modes or the approximate long-axis orientation of the area with reflectivity of ≥40 dBZ in the NL mode. Hourly ERA5 data at immediate maturation times for the top three modes were chosen to analyze the prestorm wind fields. The motion of each storm is calculated by the distance of the geometric centers of the regions with reflectivity of ≥40 dBZ from 1 h immediately before the maturation time to the maturation time observed in the radar images.

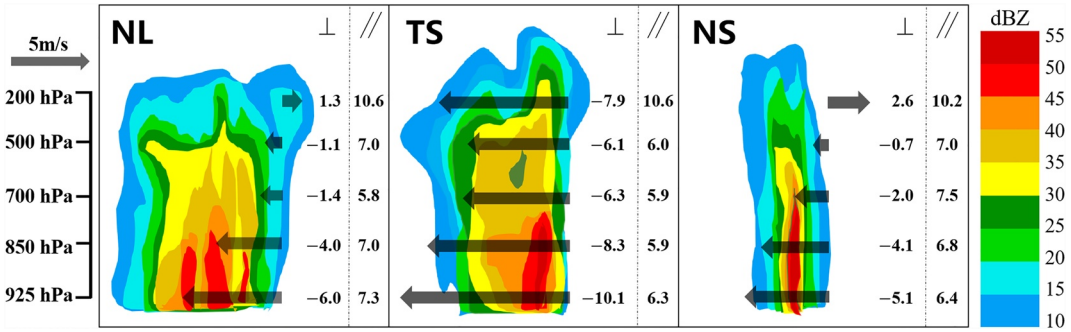

Figure 12. Vertical cross-sections of the top three organizational modes and associated storm-relative prestorm winds. The "⊥" symbols and arrows indicate the components of the storm-relative prestorm winds perpendicular to the orientation of the mesoscale convective system (MCS), with negative values representing the rearward components and positive values representing the forward components. The "//" symbols represent the absolute values of the components parallel to the orientation of the MCS. The numbers denote the perpendicular components of the storm-relative prestorm winds and the absolute values of the parallel components.

The results show that the TS mode has apparently larger rearward storm-relative wind in the middle–upper layer than do the NL and NS modes (Figure 12) and thus can explain the trailing stratiform precipitation (Dalal et al., 2012; Parker & Johnson, 2000). The rearward storm-relative wind observed in systems of the TS mode is favorable for hydrometeors to appear behind the convective line. The line-perpendicular storm-relative winds are much smaller in the middle–upper level (500 and 200 hPa) of systems of the NL and NS modes than those observed in systems of the TS mode and are much smaller than their line-parallel components; this result is consistent with the much smaller stratiform precipitation seen in systems of the NS mode and the lack of consistent preference of stratiform rainfall in their locations in systems of the NL mode.

5. Precipitation Characteristics of Different Organizational Modes

One-, 3-, and 6-h rainfall features were examined for various organizational mode. Among the top three most frequent organizational modes, the NL mode produces the highest 3- and 6-h maximum precipitation values (Table 4), which are significantly larger than those of the TS and NS modes at a significance level of over 90%, and a higher hourly maximum precipitation value than that of the NS mode at the 91% significance level (Student's *t*-test was used to analyze the differences in rainfall amounts among the different organizational modes). The NL mode produces 97.2-mm 3-h maximum precipitation values and 117.8-mm 6-h maximum precipitation values, which are much larger than those of the TS and NS modes; this result is possibly associated with the slower movements of systems of the NL mode, as mentioned in Section 3.3. On average, the NL mode produces 53.9-mm hourly maximum precipitation values with two NL cases even exceeding 100 mm, while the TS and NS modes produce 45.8- and 40.6-mm hourly maximum precipitation values on average, respectively.

Among all organizational modes, the EL mode produces the highest average 1-, 3-, and 6-h maximum precipitation values, agreeing with the statistical results which show that the EL mode is the most effective in

Table 4
Average 1-, 3-, and 6-h Maximum Precipitation Values of Different Organizational Modes

Precipitation (mm)	NL	TS	NS	EL	MRB	BE	PS	TL/AS	LS
1-h	53.9	45.8	40.6	91.4	50.8	68.3	68.2	45.7	59.1
3-h	97.2	70.7	62.3	148.2	92.1	102.1	102.6	84.3	95.9
6-h	117.8	79.2	75.4	208.5	146.5	121.6	118.4	108.3	108.0

Note. BE, bow echoes; EL, embedded lines; LS, leading stratiform precipitation; MRB, multiple rain bands; NS, no stratiform precipitation; NL, nonlinear mode; PS, parallel stratiform precipitation; TS, trailing stratiform precipitation; TL/AS, training line/adjoining stratiform.

producing short-term intense precipitation over central East China (Zheng et al., 2013), while the TS and NS modes produce the lowest 6-h precipitation values, with the TS mode values being slightly larger than the NS mode values. The NL mode produces lower 6-h maximum precipitation than do the EL, MRB, BE, and PS modes but higher 6-h maximum precipitation than do the TL/AS and LS modes, as shown in Table 4.

6. Summary

Warm-sector rainfall in South China, which is a very special type of disastrous weather under the condition of weak synoptic-scale forcing, having fewer occurrences than frontal rainfall but producing much more localized, heavier precipitation with much lower QPF skills and thus having been a big challenge in operational forecast. Understanding the morphologies of the MCSs associated with warm-sector rainfall in South China, which has not received adequate attention, is crucial for forecasting this special type of heavy rainfall.

This work examined the organizational features of MCSs associated with warm-sector heavy rainfall and their environmental features during April–June from 2007 to 2020 in South China. A total of 92 MCS cases were identified and classified into nine organizational modes, including the NL and eight linear modes: the NS, EL, TS, BE, LS, PS, TL/AS, and MRB modes. The proportions of the different organizational modes are as follows: NL (40%), TS (24%), NS (13%), TL/AS (6%), LS (5%), MRB (5%), EL (3%), PS (2%), and BE (2%). The top three most frequently observed organizational modes are the NL, TS, and NS modes, which are different from central East China where the most frequent modes are the NL, EL, and NS due to different synoptic environments generally in strong synoptic-scale forcing such as cold fronts or Mei-yu fronts. This work mainly examined the general features of the top three most frequently observed organizational modes in detail.

Most MCSs associated with warm-sector heavy rainfall events appear in June with apparent diurnal variations. The MCSs display an early morning (2300–0200 BJT) and early afternoon peak (1100–1400 BJT) in their initiation times and a morning peak (0800–1100 BJT) in their maturation times. The early morning initiation peak and the morning maturation peak of all MCSs are also shown in those of the NL mode. Most NL systems take 5–7 h to reach maturity, which is significantly shorter than that of linear systems. Nearly 77% of MCSs associated with warm-sector heavy rainfall in South China persist for 5–20 h. The average lifespan of linear systems is significantly longer than that of NL systems.

Most MCSs are initiated along the coastlines of Guangdong and Guangxi Provinces. The major concentrated center of initiation locations of all MCSs is located in Yangjiang city, and the minor concentrated centers are located in Fangchenggang and Beihai cities. Fifty-nine percent of systems of the NL mode, 63% of those of the TS mode, and 75% of NS systems form near coastlines. Most systems of the NL and TS modes move northeastward. Of all NS systems, 33%, 33%, and 25% move north, northeast, and stay quasi-static, respectively. The NL mode contributes the most to MCSs with quasi-static movements. The maturation locations show two concentrated centers, one of which is slightly east of the minor concentrated center of initiation locations in Fangchenggang city, while the other is located obviously east of the major concentrated center of initiation locations in the Pearl River Delta. The maturation locations of TS and NS systems are obviously east of their initiation locations, while the maturation locations of NL systems are similar to their initiation locations, which is consistent with their slow movements.

The MCSs associated with warm-sector heavy rainfall in South China form mainly via the broken areal mode. In particular, 84% of NL systems and 77% of TS systems form via the broken areal mode, while 83% of NS systems form via the broken line mode. The top three organizational modes dissipate mainly via the segmenting mode. Only 16% of NL systems, 9% of TS systems, and 17% of NS systems dissipate via the shrinking mode.

The results showed significant differences in the environmental parameters of the 0–3-km vertical wind shear, 0–6-km vertical wind shear, relative humidity at the low-level layers (925, 850 hPa), TTI, MUCAPE, MUCIN, and LI among some organizational modes. Among the top three most frequent organizational modes, the TTI is the key factor in differentiating all the top three organizational modes. The TTI is the largest in the TS mode, the smallest in the NS mode, and is intermediate in the NL mode with statistical

significance. Significant differences were found among some of the top three modes in other parameters. The 0–3-km (or 6-km) wind shear in the NS mode is significantly smaller than those in the NL and TS modes. The relative humidity values at 925 and 850 hPa in the NL mode are significantly larger than those in the TS mode. The MUCAPE and MUCIN values and the absolute value of LI in the TS mode are significantly higher than those in the NL and NS modes. In addition, the prestorm storm-relative wind shows that the TS mode has apparently larger rearward line-perpendicular storm-relative wind in the middle–upper layer than do the other two modes. NL and NS systems exhibit dominant line-parallel storm-relative wind in the middle–upper layer. Our results on the environmental features of NL modes and their differences from other modes complement previous works which mainly focused on the environmental features of linear modes (e.g., Zheng et al., 2013).

The NL mode is more effective than the TS and NS modes are in producing 3- and 6-h maximum precipitation values, possibly due to the slower movements of systems of the NL mode. The NL mode produces a significantly higher hourly maximum precipitation value than that of the NS mode. The EL mode produces the highest 1-, 3-, and 6-h maximum precipitation values among all nine organizational modes associated with warm-sector heavy rainfall, while the NS mode produces the lowest precipitation values.

One limitation of the present study is the relatively small sample size of the morphologies of MCSs associated with warm-sector heavy rainfall events in South China. The small sample size is due to the following reasons. (a) Our target systems are MCSs that are associated with warm-sector heavy rainfall events, which occur without fronts or at least 200 km ahead of fronts in South China. This special type of event has fewer occurrences than frontal rainfall events but produces much more localized, heavier precipitation with much lower QPF skills and thus is in urgent need of understanding. For example, according to Wu, Ding, et al. (2020), there were a total of 191 heavy rainfall days during April–June from 2003 to 2014 in Guangdong Province, covering 48 warm-sector rainfall-only days, 125 front-only days, and 18 days of both warm-sector and front days. To make a clear-cut study, we also removed the cases where the frontal-rainfall-associated MCSs merged with warm-sector heavy-rainfall-associated MCSs during the whole lifespan of each of the warm-sector heavy-rainfall-associated MCSs. (b) We focused on the morphologies of MCSs at maturation time when the most intense rainfall was produced rather than all the morphologies during the whole lifecycle of each MCS. Even though the sample size is not quite large, statistical significance testing has been performed for all presented differences between different organizational modes to make our statistical results credible. These results could become important references for operational forecasting of warm-sector heavy rainfall.

Data Availability Statement

Radar data and hourly precipitation data were provided by the National Meteorological Center of the China Meteorological Administration (available online at http://www.nmc.cn/publish/radar/huanan.html, and https://data.cma.cn/data/cdcdetail/dataCode/A.0012.0001.html). The ERA5 reanalysis data were downloaded from https://cds.climate.copernicus.eu/cdsapp#!/dataset/reanalysis-era5-pressure-levels?tab=overview and https://cds.climate.copernicus.eu/cdsapp#!/dataset/reanalysis-era5-single-levels?tab=overview. Hersbach et al. (2018a, 2018b) were downloaded from the Copernicus Climate Change Service (C3S) Climate Data Store.

Acknowledgments
This work was supported by the Natural Science Foundation of China (Grants 42030604, 41875051, 41425018, and 41461164006).

References

Bai, L., Chen, G., & Huang, L. (2020). Convection initiation in monsoon coastal areas (South China). *Geophysical Research Letters*, *47*. https://doi.org/10.1029/2020GL087035

Blanchard, D. O. (1990). Mesoscale convective patterns of the southern High Plains. *Bulletin of the American Meteorological Society*, *71*, 994–1005. https://doi.org/10.1175/1520-0477(1990)071<0994:MCPOTS>2.0.CO;2

Bluestein, H. B., & Jain, M. H. (1985). Formation of mesoscale lines of precipitation: Severe squall lines in Oklahoma during the spring. *Journal of the Atmospheric Sciences*, *42*, 1711–1732. https://doi.org/10.1175/1520-0469(1985)042<1711:FOMLOP>2.0.CO;2

Chen, X., Ding, Z., Liu, C., Chang, Y., & Zhu, C. L. (2012). Statistic analysis on the formation systems of warm-sector heavy rainfall in May and June from 2000-2009 [in Chinese]. *Journal of Tropical Meteorology*, *28*(5), 707–718. https://doi.org/10.3969/j.issn.1004-4965.2012.05.010

Dai, A., Giorgi, F., & Trenberth, K. E. (1999). Observed and model-simulated diurnal cycles of precipitation over the contiguous United States. *Journal of Geophysical Research*, *104*, 6377–6402. https://doi.org/10.1029/98JD02720

Dalal, S., Lohar, D., Sarkar, S., Sadhukhan, I., & Debnath, G. C. (2012). Organizational modes of squall-type mesoscale convective systems during premonsoon season over eastern India. *Atmospheric Research*, *106*, 120–138. https://doi.org/10.1016/j.atmosres.2011.12.002

Ding, Y. (1994). *Monsoons over China* (p. 419). Kluwer Academic Publishers.

Ding, Z., Liu, C., & Shen, X. (2011). Statistical analysis of the relationship among warm sector heavy rainfall, upper and lower tropospheric jet stream and South Asia high in May and June from 2005 to 2008 [in Chinese]. *Journal of Tropical Meteorology*, *27*(3), 307–316. https://doi.org/10.3969/j.issn.1004-4965.2011.03.003

Duda, J. D., & Gallus, W. A., Jr. (2010). Spring and summer midwestern severe weather reports in supercells compared to other morphologies. *Weather and Forecasting*, *25*(1), 190–206. https://doi.org/10.1175/2009WAF2222338.1

Gallus, W. A., Jr, Snook, N. A., & Johnson, E. V. (2008). Spring and summer severe weather reports over the Midwest as a function of convective mode: A preliminary study. *Weather and Forecasting*, *23*(1), 101–113. https://doi.org/10.1175/2007waf2006120.1

He, L., Chen, T., & Kong, Q. (2016). A review of studies on prefrontal torrential rain in South China. *Journal of Applied Meteorological Science*, *27*(5), 559–569. https://doi.org/10.11898/1001-7313.20160505

Hersbach, H., Bell, B., Berrisford, P., Biavati, G., Horányi, A., Muñoz Sabater, J., et al. (2018a). *ERA5 hourly data on pressure levels from 1979 to present*. Copernicus Climate Change Service (C3S) Climate Data Store (CDS). https://doi.org/10.24381/cds.bd0915c6

Hersbach, H., Bell, B., Berrisford, P., Biavati, G., Horányi, A., Muñoz Sabater, J., et al. (2018b). *ERA5 hourly data on single levels from 1979 to present*. Copernicus Climate Change Service (C3S) Climate Data Store (CDS). https://doi.org/10.24381/cds.adbb2d47

Huang, S. S., Li, Z., Bao, C., Yu, Z., Chen, H., Yu, S., et al. (1986). *Heavy rainfall over southern China in early-summer rainy season [in Chinese]* (p. 244). Guangdong Science and Technology Press.

Jirak, I. L., Cotton, W. R., & Mcanelly, R. L. (2003). Satellite and radar survey of mesoscale convective system development. *Monthly Weather Review*, *131*(10), 2428–2449. https://doi.org/10.1175/1520-0493(2003)131<2428:SARSOM>2.0.CO;2

Kruskal, W. H., & Wallis, W. A. (1952). Use of ranks in one-criterion variance analysis. *Journal of the American Statistical Association*, *47*(260), 583–621. https://doi.org/10.2307/2280779

Liang, Q., Xiang, S., Lin, L., & Meng, W. G. (2012). MCS characteristics over South China during the annually firstly rainy season and their organization types [in Chinese]. *Journal of Tropical Meteorology*, *28*(04), 541–551. https://doi.org/10.3969/j.issn.1004-4965.2012.04.013

Liang, Z., Fovell, R. G., & Liu, Y. (2019). Observational analysis of the characteristics of the synoptic situation and evolution of the organized warm-sector rainfall in the coastal region of South China in the pre-summer rainy season. *Atmosphere*, *10*(11), 722. https://doi.org/10.3390/atmos10110722

Lin, L. (2006). *Guangdong weather forecast technical manual* (pp. 119–150). Meteorological Press.

Liu, R., Sun, J., & Chen, B. (2019). Selection and classification of warm-sector heavy rainfall events over South China [in Chinese]. *Chinese Journal of Atmospheric Sciences*, *43*(1), 119–130. https://doi.org/10.3878/j.issn.1006-9895.1803.17245

Liu, X., Luo, Y., Guan, Z., & Zhang, D.-L. (2018). An extreme rainfall event in coastal South China during SCMREX-2014: Formation and roles of Rainband and Echo trainings. *Journal of Geophysical Research: Atmospheres*, *123*, 9256–9278. https://doi.org/10.1029/2018JD028418

Loehrer, S. M., & Johnson, R. H. (1995). Surface pressure and precipitation life cycle characteristics of PRE-STORM mesoscale convective systems. *Monthly Weather Review*, *123*(3), 600–621. https://doi.org/10.1175/1520-0493(1995)123<0600:SPAPLC>2.0.CO;2

Lombardo, K. A., & Colle, B. A. (2011). Convective storm structures and ambient conditions associated with severe weather over the Northeast United States. *Weather and Forecasting*, *26*(6), 940–956. https://doi.org/10.1175/WAF-D-11-00002.1

Luo, Y. (2017). Advances in understanding the early-summer heavy rainfall over South China. In C.-P. Chang, et al. (Eds.), *The Global Monsoon System* (3rd ed., pp. 215–226). World Scientific. https://doi.org/10.1142/9789813200913_0017

Luo, Y., Zhang, R., Wan, Q., Wang, B., Wong, W. K., Hu, Z., et al. (2017). The Southern China Monsoon Rainfall Experiment (SCMREX). *Bulletin of the American Meteorological Society*, *98*(5), 999–1013. https://doi.org/10.1175/bams-d-15-00235.1

Meng, Z., Yan, D., & Zhang, Y. (2013). General features of squall lines in East China. *Monthly Weather Review*, *141*(5), 1629–1647. https://doi.org/10.1175/MWR-D-12-00208.1

Parker, M. D. (2007). Simulate convective lines with parallel stratiform precipitation. Part I: An archetype for convective in along-line shear. *Journal of the Atmospheric Sciences*, *64*(2), 267–288. https://doi.org/10.1175/JAS3853.1

Parker, M. D., & Johnson, R. H. (2000). Organizational modes of midlatitude mesoscale convective systems. *Monthly Weather Review*, *128*(10), 3413–3436. https://doi.org/10.1175/1520-0493(2001)129<3413:OMOMMC>2.0.CO;2

Schumacher, R. S., & Johnson, R. H. (2005). Organization and environmental properties of extreme-rain-producing mesoscale convective systems. *Monthly Weather Review*, *133*(4), 961–976. https://doi.org/10.1175/MWR2899.1

Schumacher, R. S., & Peters, J. M. (2017). Near-surface thermodynamic sensitivities in simulated extreme-rain-producing mesoscale convective systems. *Monthly Weather Review*, *145*(6), 2177–2200. https://doi.org/10.1175/MWR-D-16-0255.1

Squitieri, B. J., & Gallus, W. A. (2016). WRF forecasts of great plains nocturnal low-level jet-driven MCSs. Part I: Correlation between low-level jet forecast accuracy and MCS precipitation forecast skill. *Weather and Forecasting*, *31*(4), 1301–1323. https://doi.org/10.1175/WAF-D-15-0151.1

Sun, J., Zheng, L., & Zhao, S. (2014). Impact of moisture on the organizational mode and intensity of squall lines determined through numerical experiments [in Chinese]. *Chinese Journal of Atmospheric Sciences*, *38*(4), 742–755. https://doi.org/10.3878/j.issn.1006-9895.2013.13187

Wang, H., Luo, Y., & Jou, B. J.-D. (2014). Initiation, maintenance, and properties of convection in an extreme rainfall event during SCMREX: Observational analysis. *Journal of Geophysical Research: Atmospheres*, *119*(23), 13206–13232. https://doi.org/10.1002/2014jd022339

Wang, X., Cui, C., Cui, W., & Shi, Y. (2014). Modes of mesoscale convective system organization during Meiyu season over the Yangtze River basin. *Journal of Meteorological Research*, *28*(1), 111–126. https://doi.org/10.1007/s13351-014-0108-4

Weisman, M. L. (2001). Bow echoes: A tribute to T. T. Fujita. *Bulletin of the American Meteorological Society*, *82*(1), 97–116. https://doi.org/10.1175/1520-0477(2001)082<0097:beattt>2.3.co;2

Wilcoxon, F. (1945). Individual comparisons by ranking methods. *Biometric Bulletin*, *1*(6), 80–83. https://doi.org/10.2307/3001968

Wu, M., & Luo, Y. (2016). Mesoscale observational analysis of lifting mechanism of a warm-sector convective system producing the maximal daily precipitation in China mainland during pre-summer rainy season of 2015. *Journal of Meteorological Research*, *30*(5), 719–736. https://doi.org/10.1007/s13351-016-6089-8

Wu, N., Ding, X., Wen, Z., Chen, G., Meng, Z., Lin, L., & Min, J. (2020). Contrasting frontal and warm-sector heavy rainfalls over South China during the early-summer rainy season. *Atmospheric Research*, *235*, 104693. https://doi.org/10.1016/j.atmosres.2019.104693

Wu, N., Zhuang, X., Min, J., & Meng, Z. (2020). Practical and intrinsic predictability of a warm-sector torrential rainfall event in the South China monsoon region. *Journal of Geophysical Research: Atmospheres*, *125*(4), https://doi.org/10.1029/2019JD031313

Yang, X., & Sun, J. (2018). Organizational modes of severe wind—Producing convective systems over North China [J]. *Advances in Atmospheric Sciences*, *35*(5), 540–549. https://doi.org/10.1007/s00376-017-7114-2

Yu, R., Zhou, T., Xiong, A., Zhu, Y., & Li, J. (2007). Diurnal variations of summer precipitation over contiguous China. *Geophysical Research Letters*, *34*(1), 223–234. https://doi.org/10.1029/2006GL028129

Zhang, M., & Meng, Z. (2019). Warm-sector heavy rainfall in Southern China and its WRF simulation evaluation: A low-level-jet perspective. *Monthly Weather Review*, *147*(12), 4461–4480. https://doi.org/10.1175/MWR-D-19-0110.1

Zheng, L., Sun, J., Zhang, X., & Liu, C. (2013). Organizational modes of mesoscale convective systems over Central East China. *Weather and Forecasting*, *28*(5), 1081–1098. https://doi.org/10.1175/WAF-D-12-00088.1

Zhou, T., Yu, R., Chen, H., Dai, A., & Pan, Y. (2008). Summer precipitation frequency, intensity, and diurnal cycle over China: A comparison of satellite data with rain gauge observations. *Journal of Climate*, *21*(16), 3997–4010. https://doi.org/10.1175/2008JCLI2028.1